Research Article

Humberto Peredo Fuentes*

Application of the mode-shape expansion based on model order reduction methods to a composite structure

https://doi.org/10.1515/eng-2017-0026
Received Jul 09, 2016; accepted May 31, 2017

Abstract: The application of different mode-shape expansion (MSE) methods to a CFRP based on model order reduction (MOR) and component mode synthesis (CMS) methods is evaluated combining the updated stiffness parameters of the full FE model obtained with a mix-numerical experimental technique (MNET) in a previous work. The eigenvectors and eigenfrequencies of the different MSE methods obtained are compared with respect to the experimental measurements and with a full FE model solutions using the modal assurance criteria (MAC). Furthermore, the stiffness and mass weighted coefficients (K-MAC and M-MAC respectively) are calculated and compared to observe the influence of the different subspace based expansion methods applying the MAC criteria. The K-MAC and M-MAC are basically the MAC coefficients weighted by a partition of the global stiffness and mass matrices respectively. The best K-MAC and M-MAC results per paired mode-sensor are observed in the subspace based expansion MODAL/SEREP and MDRE-WE methods using the updated stiffness parameters. A strong influence of the subspace based on MOR using MSE methods is observed in the K-MAC and M-MAC criteria implemented in SDTools evaluating the stiffness parameters in a contrieved example.

Keywords: Composites, Mode-shape expansion, GUYAN, MODAL, SEREP, DYNAMIC, MDRE, MDRE-WE, MAC, K-MAC, M-MAC

1 Introduction

The concept of mode-shape expansion (MSE), model order reduction (MOR) and component mode synthesis (CMS) methods play a significant role in the dynamic analysis of conventional materials or carbon fiber reinforced polymer (CFRP), especially comparing large analytical set of degree of freedom (DOF) versus experimental models with relatively small number of sensors [1–34]. The experimental measurements (EM) are critical for the success of any structural dynamic analysis and contain characteristics that cannot be obtained analytically [1]. Traditionally, interface model reductions [1–3, 5–9, 29] are used to estimate the motion at interfaces DOFs by the motion of sensors using EM, where the EM played a significant role in the correlation and updating of analytical models. Many approaches to correlate analytical models require measured vectors to be available at the full set of finite element DOF. Likewise, model updating in the set of tested DOF requires the large model to be reduced to a much smaller size but without distortion of the reduced model. Coupled predictions can also be estimated using MSE methods [1]. Two groups can basically be distinguished to characterize coupled predictions: unmodified structures, see [5] for further details, and modified structures illustrated in [1–3, 5–9, 29]. The difference between the two groups is basically that the first group needed to impose some of the measurement points on the interface while in the second group, it is not needed. The methodology presented by Corus *et al.* in [6] and Balmès [1–3, 8, 9, 29] combined techniques offering the advantages of the second group of coupled predictions consisting of: a local FE model, classical theory of structural modification by coupling it with MSE and CMS with several interface MOR methods (subspace selection) [1–3, 8]. The use or not of modifications in this methodology [1] is distinguished as an indicator for the validity of coupled predictions. The MSE methodology concept is used in this work to estimate the responses of all degrees of freedom of the interface of a CFRP component defined by the motion of sensors evaluating the stiffness parameters of a full finite element (FE) model obtained in [10]. The accuracy of the experimental measurements obtained in [10] and verified in [11] using discrete Kirchhoff triangular (DKT) elements including transversal shear effects [26], also know as discrete shear triangular (DST) [27, 28] and a reduced finite element model using superlements

*Corresponding Author: Humberto Peredo Fuentes: Institute of Mechanics, Technical University Berlin, Strasse des 17. Juni 135, 10623 Berlin, Germany; Email: hperedo@mailbox.tu-berlin.de

applying the Craig-Bampton model order reduction based in Ritz vectors defined in [29]. Different advance interpolation MSE methods implemented in [29] are performed to determine the coupled predictions in the CFRP component such as: MODAL [12], SEREP [13], STATIC (based on Guyan reduction [14]), DYNAMIC [15], minimum residual dynamic expansion (MRDE) [16], and minimum residual dynamic expansion with test-error (MRDE-WE) [17]. The MRDE and MRDE-WE are also known as hybrid methods. The MSE methods are calculated using EM, curve-fitting algorithms, and a FE model to obtain the interpolation results. Thus, these advance MSE interpolation methods can be evaluated to determine the paired accuracy predictions in the CFRP component for unmeasured DOFs in a CFRP component applying the modal assurance criterion [19] (MAC) based on the EM, the curve-fitting algorithms, and the updated stiffness parameters of the full FE model obtained with a MNET. The impact of the accuracy in the results using MSE is documented in the literature for conventional materials taking in consideration residual modes [18]. The application of these MSE methods and it's accuracy to a CFRP is not documented in the literature. The influence of the MOR applying MSE methods implemented in [29] is evaluated using the stiffness and mass weighted criteria or K-MAC and M-MAC (normalized stiffness and mass cross-orthogonality criteria respectively) based on the MAC. In section 2, it is introduced a brief theoretical background of this MSE methodology developed by Corus and Balmès. In section 3, the results are discussed based on the updated stiffness parameters obtained of the FE model versus the modification of these stiffness parameters (contrieved example). The conclusions are discussed in section 4.

2 Theoretical background

Initially, the theoretical background of the MSE methodologies combining different techniques introduced in [1, 2, 4, 6, 9, 29] was established as a close loop prediction problem for structural modifications. The knowledge of the close loop prediction problem between the physical and the analytical model is used in the industry applying experimental measurements and the finite element method (FEM) to reduce the cost of prototypes components. A number of steps are described in [29] such as: EM, curve-fitting algorithms, laminate theory, form of the lineal differential equation, dealing with continuous interfaces and the evaluation of the error. These steps are briefly introduced and adapted for the objective of this work in the next sections.

2.1 Experimental measurements

The experimental measurements described by the frequency response functions (FRF). $H(\omega_i)$, is defined as the ratio of the transformed excitation [19]:

$$H(\omega_i) = \frac{X(\omega_i)}{F(\omega_i)}, \tag{1}$$

where $H(\omega_i)$ is the measured (predicted) FRF transfer function matrix, $X(\omega_i)$ the Fourier spectrum of response, and $F(\omega_i)$ is the Fourier spectrum of excitation force. The FRF in Eq. (1) is the inverse of the dynamic stiffness:

$$H(\omega_i) = \left[-\omega_i^2[M] + \omega_i[C] + [K]\right]^{-1}, \tag{2}$$

where the mass $[M]$, damping $[C]$ and stiffness $[K]$ matrices in Eq. (2) are dependent of physical parameters such as material's density, Young's and shear moduli and Poisson's ratio [10].

2.2 Curve-fitting Algorithms

The goal of using the curve-fitting algorithms is to produce an accurate estimation of the modal parameters of the CFRP component using the FRF. There are several methods that can be used to estimate the modal parameters based on one mode at a time (SDOF) or more modes at a time (MDOF, global and multi-reference) [30]. The global curve-fitting expression called the rational fraction polynomial (RFP) or partial fraction expansion (PFE) is received with great interest and attention for its simplicity and easy implemention in personal computers (PC) [31] for the last 20 years [32–34]. The RFP form of poles and residues, illustrated in Eq. (3), offers advantages over other forms documented in literature [30, 31, 34].

$$H(s) = \sum_{k=1}^{modes} \left(\frac{[R_k]}{s - \lambda_1} + \frac{[R_k^\star]}{s - \lambda_2^\star} \right) \tag{3}$$

The residue matrices $[R_k]$ and $[R_k^\star]$ are defined as the constant numerators of the transfer function matrix, "modes" are the number of modes of vibration, λ_r is the pole location and (s) is the Laplace variable. The RFP form in Eq. (3) is typically used when the modal data is obtained from experimental transfer function measurements (FRF's). Traditionally the relationship between residues and mode shapes are expressed in terms of FRF or modal parameters. The identification of experimental measurements is determined obtaining modes whose poles are located in the test frequency range selected. A characteristic of the curve-fitting algorithms *identification De Résidus*

Complexes (IDRC) and *Identification De Résidus Multiples* (IDRM) used in this work are the residual terms $[R_k(\lambda_r)]$, $[E(s)]$ and $[F(s)]$ defined in [21]. The contributions of the residual terms in the transfer functions are used to evaluate the high and low frequency mode terms respectively, see Eq. (4).

$$H(s) = \sum_{k=1}^{modes} \left(\frac{[R_k]}{s-\lambda_1} + \frac{[R_k^\star]}{s-\lambda_2^\star} \right) + [E(s)] + \frac{[F(s)]}{s^2} \quad (4)$$

The residual terms are known also a residual modes or residual vectors [21] and it is documented the advantages of the application of the residual terms in the literature [18]. Thus, the estimation of the poles depends linearly on the residual terms $[R_k(\lambda_r), E(s), F(s)]$ solving the linear least squares problem associated with the frequency domain output error illustrated in Eq. (5).

$$\left[R_k(\lambda_r), E(s), F(s)\right] = arg\ min\ \left|[H(s)]_{test} - H(s)\right|^2 \quad (5)$$

where the residue matrix $[R_k] = \{c\phi_j\}\{\phi_j^T b\}$ is given by the product of a column observability $\{c\phi_j\}$ and row controllability $\{\phi_j^T b\}$ defined in [21]. The residue matrix $[R_k]$ is often expressed as $[A_j] = \{\phi_j\}\{L_j\}$ in the structural dynamics community, where $[A_j]$ is commonly called *modal participation factor*, $\{\phi_j\}$ is the modeshape and $\{L_j\}$ is the controllability [29]. Assuming that the complex poles come in conjugate pairs and the residue matrices too, the normal mode residue with symmetric pole structure can be defined as a rational fraction expression (to determine the damping ratios that are different for each pole using the normal mode model format proposed by Balmès in [21] of the form:

$$H(s) = \sum_{j=1}^{N} \frac{\{[c]\phi_j\}\{\phi_j^T[b]\}}{s^2 + 2\zeta_j\omega_j s + \omega_j^2} = \sum_{j=1}^{N} \frac{[T_j]}{s^2 + 2\zeta_j\omega_j s + \omega_j^2} \quad (6)$$

where the contribution of each mode is characterized by the pole frequency ω_j, damping ratio ζ_j, and the normal mode residues matrix $[T_j]$ with symmetric pole structure [21]. The matrix $[T_j]$ is equal to the product of the normal mode output shape matrix $\{[c]\phi_j\}$ by the normal mode input shape matrix $\{[b]\phi_j^T\}$. The matrix $[b]$ is called the input shape matrix and the matrix $[c]$ is called the output shape matrix. This matrix description is established based on several assumptions in [29] and it can be applied considering second order models of the form introduced in subsection 2.4.

2.3 Laminate Theory

The classical laminate theory (CLT) and the first-order shear deformation laminate theory (FSDT) are applicable to linear and composite elastic materials [26], by means of the Discrete Mindlin Kirchhoff Triangle (DMKT) elements also known as Discrete Shear Triangle (DST) elements [27, 28]. One characteristic of these triangle elements is that the Mindlin/Reissner plate theory can be reduced theoretically to the Kirchhoff plate theory if the transverse shear effects are not important [28]. These laminate theories have been used extensively to predict elastic behavior of the traditional fiber-reinforced polymers (FRP). FRP materials (carbon or glass FRP) are widely used in aerospace and construction applications. One important consideration is to have perfectly bonded layers with a uniform thickness (see Figure 1). The mechanical properties measured in ply level experiments are used to populate the stiffness matrix for each ply. The stiffness matrices for the individual plies are combined to form the laminate stiffness matrix $ABD-\tilde{S}$ in:

$$\begin{Bmatrix} N_i \\ M_i \\ S_{ij} \end{Bmatrix} = \begin{bmatrix} A & B & 0 \\ B & D & 0 \\ 0 & 0 & \tilde{S} \end{bmatrix} \begin{Bmatrix} \epsilon_i \\ \kappa_i \\ \gamma_{ij} \end{Bmatrix}. \quad (7)$$

The $ABD-\tilde{S}$ matrix in Eq. (7) relates forces (N_i), moments

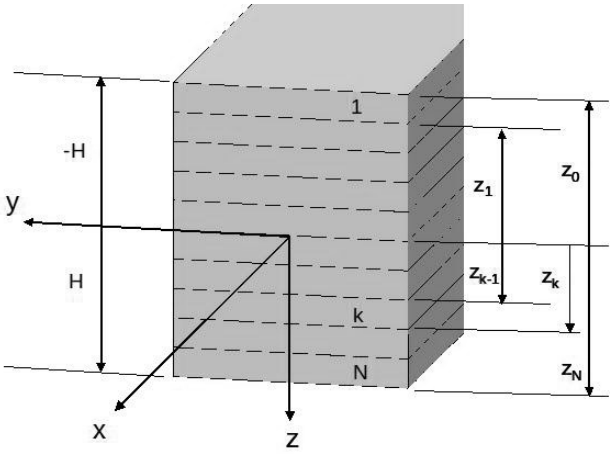

Figure 1: Configuration of composite layers [10].

(M_i) and shear stresses (S_{ij}) to strains (ϵ_i), curvatures (κ_i) and shear strains (γ_{ij}). The components of the $ABD-\tilde{S}$ matrix are given in Eqs. (8)-(11), where N is the number of plies, $[Q_k]$ is the stiffness matrix of each ply, z_k denotes the distance from the laminate's mid-plane to the edges of single plies, and K is the shear correction factor usually taken as 5/6:

$$[A] = \sum_{K=1}^{N} [\bar{Q}_k]^{(k)}(z_{k+1} - z_k), \quad (8)$$

$$[B] = \frac{1}{2}\sum_{K=1}^{N}[\bar{Q}_k]^{(k)}(z_{k+1}^2 - z_k^2), \tag{9}$$

$$[D] = \frac{1}{3}\sum_{K=1}^{N}[\bar{Q}_k]^{(k)}(z_{k+1}^3 - z_k^3), \tag{10}$$

$$[\tilde{S}] = K\sum_{K=1}^{N}[\bar{Q}_k]^{(k)}(z_{k+1} - z_k), \tag{11}$$

2.4 Form of the linear differential equation

It is considered only second order models of the form, see [10] and [29], and reintroduced in this section to perform MSE to a composite component assembly) in Eq. (12):

$$\left[[M]s^2 + [C]s + [K]\right]_B \{q_B(s)\} = [b_{IB}]\{u_{IB}(s)\} \qquad \{y_{IB}(s)\} = [c_{IB}]\{q_B(s)\} \tag{12}$$

where (s) is the Laplace variable, $[M]$, $[C]$, $[K]$ are the mass, damping and stiffness matrices, respectively, $\{q_B(s)\}$ are the generalised degrees of freedom (DOFs) of the base, $[b_{IB}]$ and $[c_{IB}]$ are the input and output matrices of the base interface, respectively, $\{u_{IB}(s)\}$ are the inputs describing the time/frequency dependence, and $\{y_{IB}(s)\}$ are the physical outputs of the base interface defined in [1–3, 5–9, 21, 29]. Note that the input/output shape matrix formalism decouples the choice of DOF $\{q_B(s)\}$ from the choice of $\{u_{IB}(s)\}$ and $\{y_{IB}(s)\}$ [1]. The $[b_{IB}]$ and $[c_{IB}]$ are Boolean matrices of the base interface of the full FE models with compatible interface meshes. Considering the response of an elastic structure to applied loads $F(s) = [b_{IB}]\{u_{IB}(s)\}$, the exact response at a given frequency $[H(s)]$ is given in Eq. (13) by:

$$[H(s)] = [c_{IB}]\left[[M]s^2 + [C]s + [K]\right]_B^{-1}[b_{IB}] = [c_{IB}]\left[Z_B(s)\right]^{-1}[b_{IB}], \tag{13}$$

where $[Z(s)]$ is the dynamic stiffness. The interest of writing the transformation of the DOFs in this way, per Balmès [3], Corus [6] and Billet [1], is the easy translation of $[b_{IB}]$ and $[c_{IB}]$ denoted by IB in the subscript. For the coupled prediction in the CFRP component one assumes that the modification of the stiffness parameters can be modeled with the FE model in the base interface (denoted as IM subscript and M superscript). Thus, one can write the modification of the model in the form

$$\begin{bmatrix}\begin{bmatrix}Z_{II}^M(s)\end{bmatrix} & \begin{bmatrix}Z_{IC}^M(s)\end{bmatrix}\\ \begin{bmatrix}Z_{CI}^M(s)\end{bmatrix} & \begin{bmatrix}Z_{CC}^M(s)\end{bmatrix}\end{bmatrix}\begin{Bmatrix}\{y_{IM}(s)\}\\ q_C(s)\end{Bmatrix} = \begin{Bmatrix}\{u_{IM}(s)\}\\ \{0\}\end{Bmatrix}, \tag{14}$$

where the interface of DOFs explicitly appears as DOFs of the model, see [9]. The Division of the DOFs is divided into two groups: active or interface DOFs denoted by I in the subscript, and complementary, denoted by C in the subscript – observed in Eqs. (14) and (15). *Using the framework of Ritz methods, the coupled prediction is obtained by imposing displacement continuity on the base interface* ($\{y_{IB}(s)\} = \{y_{IM}(s)\}$), *and projecting the associated model on loads dual to the displacement subspace admissible under the continuity constrain. The projection thus combines continuity and dynamic equilibrium loads* ($\{u_{IB}(s)\} = \{u_{IM}(s)\}$). *The base model given by Eq.* (12) *and a modification described by Eq.* (14) *in [1] leads to*

$$\begin{bmatrix}[Z_B(s)] & 0\\ 0 & \begin{bmatrix}Z_{CC}^M(s)\end{bmatrix}\end{bmatrix} + \begin{bmatrix}b_{IB}(s)\\ 0\end{bmatrix}\begin{bmatrix}Z_{II}^M(s)\end{bmatrix}\begin{bmatrix}c_{IB} & 0\end{bmatrix} + \begin{bmatrix}b_{IB}(s)\\ 0\end{bmatrix}\begin{bmatrix}0 & Z_{IC}^M(s)\end{bmatrix} + \begin{bmatrix}0\\ Z_{IC}^M(s)\end{bmatrix}\begin{bmatrix}c_{IB} & 0\end{bmatrix}\begin{Bmatrix}q_B(s)\\ q_C(s)\end{Bmatrix} = F(s) \tag{15}$$

For $\{q_B(s)\}$ and $\{q_C(s)\}$ corresponding to FEM DOFs, $[b_{IB}]$ and $[c_{IB}]$ are the input and output Boolean matrices of the base interface respectively. Equation (15) corresponds to the standard assembly process established in [29]. For the applications considered in [29], the $\{q_B(s)\}$ are defined in modal coordinates and $\{q_C(s)\}$ corresponds to fixed interface modes of a Craig-Bampton model [1].

2.5 Dealing with continuous interfaces

The incompatibiliy between the discretisation of the FE model $\{y_I(s)\}$ and the experimental measurements $\{y_T(s)\}$ is documented in [1]. A highlight of this methodology assumes that exists a constant coefficient linear combination $[c_{IT}]$ relating the interface $\{y_I(s)\}$ and the test displacements $\{y_T(s)\}$ for the coupled response in Eq. (16):

$$\{y_I(s)\} \approx [c_{IT}]\{y_T(s)\}. \tag{16}$$

This relation imposes a strong constraint on the interface kinematics since $\{y_I(s)\}$ must be approximated by a subspace of basis $[T_G]$ with a dimension that is smaller than the number of sensors used. The choice of this subspace $[T_G]$, and the justification of its ability to represent the coupled response, is a key aspect proposed in [1]. The construction of a reduced interface model ($[T_G]$ subspace) is a classical extension of CMS addressed in the literature [2, 4, 29] using a Craig-Bampton type reduction of the modification where the constraint modes are replaced by the

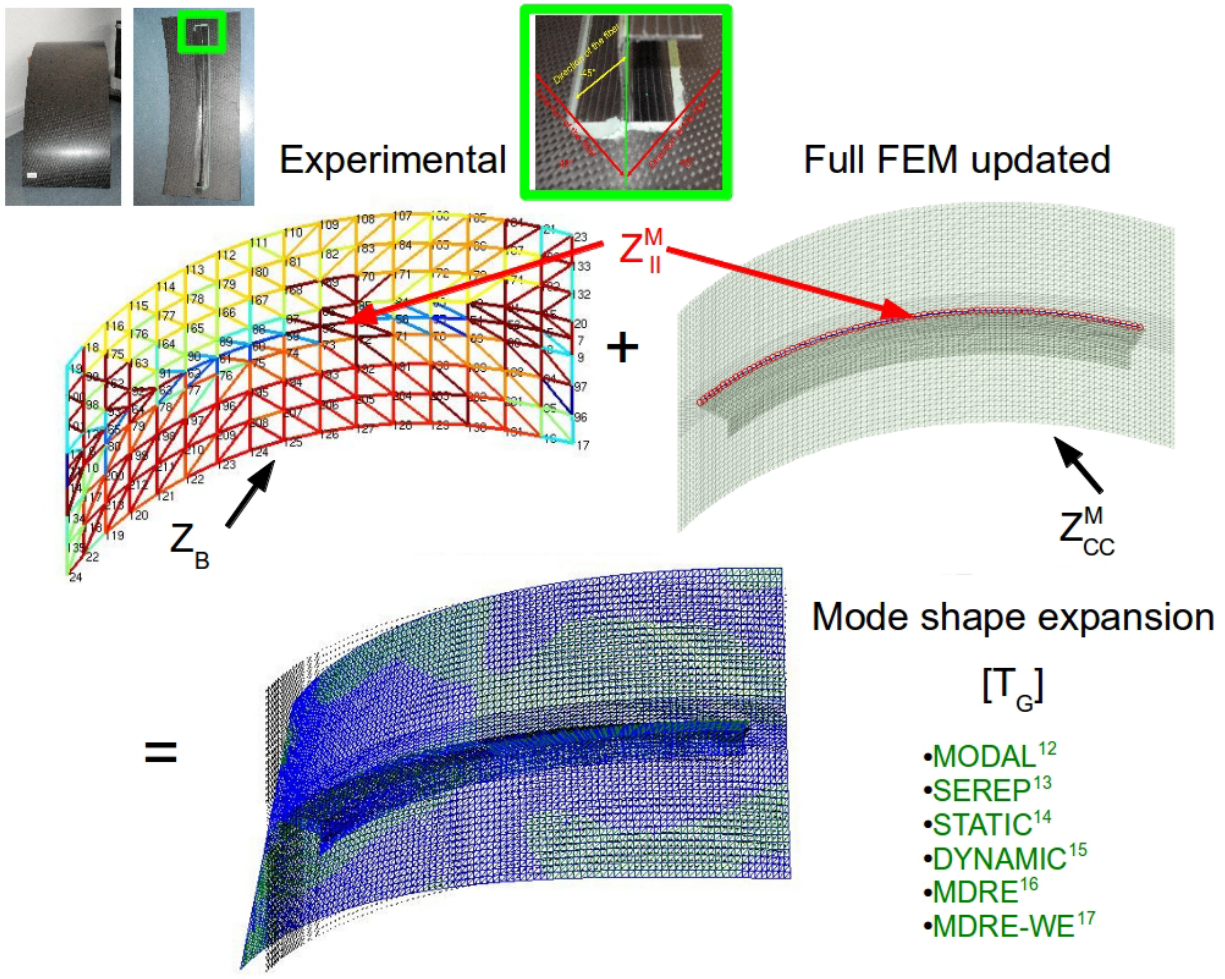

Figure 2: MSE process plot.

low order modes of the model statically condensed on its interface [1], as originally proposed in [22].

For this study, the updated FE model elaborated with triangle elements [26–28] is used to deal with the incompatibility of the interface between the FE model and the experimental measurements. The main purpose of using this updated FE model is to allow the interpolation of test motion at an arbitrary number of DOF of the interface to analyze the influence of the subspace-basis $[T_G]$ based on MOR methods in the CFRP component, (see Table 1). The subspace $[T_G]$ is defined on the DOFs of a local part of the updated FE model $[c_{IL}]$ including or not the modification, (see Figure 2).

The extraction of the interface of motion $\{y_I(s)\}$ using the updated FE model is thus written in Eq. (17) as

$$\{y_I(s)\} = [c_{IT}][T_G]\{y_G(s)\}. \tag{17}$$

An observation matrix $[T_G]$ can be constructed relating the $\{q_L(s)\}$ (DOFs of the updated FE model) with measurements $\{y_T(s)\} = [c_{TL}]\{q_L(s)\} = [c_{TG}]\{y_G(s)\} = [c_{TL}][T_G]\{y_G(s)\}$, (see [9] for possible methods). The estimation of the generalised motion of the interface $\{y_G(s)\}$, denoted by G in the subscript, can be established as:

$$\{y_G(s)\} = [c_{GB}]\{q_B(s)\}. \tag{18}$$

The standard approach to estimate the full response using different subspace-based expansion methods [1] established in [29] is then obtained by minimising the test error (distance between the test data and the associated re-

Table 1: Operator $[T_G]$ using different model order reduction methods applied to mode shape expansion methods.

MODAL/SEREP	$\{q_I(s)\}=[c_{IT}][T_G]_{MODAL/SEREP}\{y_T(s)\}$
STATIC	$\{q_I(s)\}=[c_{IT}][T_G]_{GUYAN}\{y_T(s)\}$
DYNAMIC	$\{q_I(s)\}=[c_{IT}][T_G]_{DYNAMIC}\{y_T(s)\}$
MDRE	$\{q_I(s)\}=[c_{IT}][T_G]_{MDRE}\{y_T(s)\}$
MDRE-WE	$\{q_I(s)\}=[c_{IT}][T_G]_{MDRE-WE}\{y_T(s)\}$

sponse for the expanded shape). The minimum is generally obtained by solving the least squares problem as

$$\{y_G(s)\} = \underbrace{Arg\ min}_{\{y_G\}} || [c_{TG}] \{y_G(s)\} - [c_{TB}] \{q_B(s)\} ||^2 \tag{19}$$

whose solution is given by

$$[c_{GB}] = [c_{TG}^T c_{TG}]^{-1} [c_{TG}^T c_{TB}] \tag{20}$$

which leads to the observation Eq. (16) *with* $[c_{IT}] = [c_{IL}][T_G][c_{GB}]$. *The given assumption* (17), *the second block row of Eq.* (14), *describes the motion of the modification*

$$[Z_{CC}]\{q_C(s)\} = -[Z_{CI}^M(s)][T_G]\{y_G(s)\}. \tag{21}$$

For the first block row it is assumed that the generalised loads are defined by projection on the subspace $[T_G]$ *of the form in*

$$\begin{aligned}\{u_{GM}\} = {} & [c_{IG}]^T [Z_{IC}^M(s)]\{q_C(s)\} \\ & + [c_{IG}]^T [Z_{II}^M(s)][c_{IG}]\{y_G(s)\}.\end{aligned} \tag{22}$$

The coupled response is obtained assuming dynamic equilibrium of generalised loads $\{u_{GB}\} = \{u_{GM}\}$ *established in* [1].

2.6 Evaluation of the error using the Modal Assurance Criterion (MAC)

Evaluation tools [1] are needed to evaluate the predictions based on many assumptions that introduce error. The evaluation of the error in the correlation in this study is analyzed applying a modal assurance criteria (MAC) based on the eigenfrequencies and eigenvectors divided into four parts. There are two general categories for correlation criteria: the eigenfrequencies and eigenvectors [19]. The MAC is one of the most useful comparison methods that relies on the eigenvector information, see Eq. (23) :

$$MAC = \frac{|\sum_{j=1}^{l} \{c_j\phi_{id}\}^H \{c_j\phi_k\}|^2}{|\sum_{j=1}^{l} \{c_j\phi_{id}\}^H \{c_j\phi_{id}\}|\,|\sum_{j=1}^{l} \{c_j\phi_k\}^H \{c_j\phi_k\}|}, \tag{23}$$

where $c_j\phi_{id}$ is the jth mode shape at sensors and $c_j\phi_k$ is the jth analytical mode shape. The MAC value of 1 corresponds to an absolute correlation. The less this value becomes, the worst the eigenvector correlation will be. In the modal community a MAC coefficient of a magnitude larger or equal than 0.90 in the diagonal and less or equal than 0.05 in the off-diagonal implies a satisfactory correlation. In the first part, the MAC of experimental measurements versus the updated stiffness parameters of the full FE model is analyzed. In the second part, the MSE methods are calculated to estimate the interface motion $\{y_I(s)\}$ using the experimental measurements, curve-fitting performed with the IDRC and IDRM algorithms, set-up of sensors and full FE model results. In the third part, once $\{c_j\phi_{id}\}$ and $\{c_j\phi_k\}$ are defined at sensors, it is proposed to obtain the stiffness and mass-weighted criterias, K-MAC and M-MAC, (see Eqs. (24) and (25) respectively), also called cross-generalised mass (CGM) and the less used cross-generalised stiffness (CGK) to observe the influence of the MOR using MSE methods.

The K-MAC=

$$\frac{|\sum_{j=1}^{l} \{c_j\phi_{id}\}^H [K] \{c_j\phi_k\}|^2}{|\sum_{j=1}^{l} \{c_j\phi_{id}\}^H [K] \{c_j\phi_{id}\}|\,|\sum_{j=1}^{l} \{c_j\phi_k\}^H [K] \{c_j\phi_k\}|}, \tag{24}$$

and M-MAC=

$$\frac{|\sum_{j=1}^{l} \{c_j\phi_{id}\}^H [M] \{c_j\phi_k\}|^2}{|\sum_{j=1}^{l} \{c_j\phi_{id}\}^H [M] \{c_j\phi_{id}\}|\,|\sum_{j=1}^{l} \{c_j\phi_k\}^H [M] \{c_j\phi_k\}|}, \tag{25}$$

values closer to 1 represent a higher agreement, and these values are being interpreted in the same way as the MAC [29].

The implementation of these criteria supports an original method for reducing the mass on the sensor set that used vectors defined at DOFs implemented in [29] based on the mass and stiffness matrices of the full FE model. The fourth part is evaluated modifying E_1 and E_2 equal to 97.3 GPa of all the parts defined in [10] to observe the impact of the stiffness and mass matrices in the interface motion of the full FE model applying subspace based expansion methods using the K-MACand M- MAC criteria based on the MAC.

3 Results and Discussion

The composite structure incorporates three parts, see Figures 3 and 4. The first component is made of Hunts-man

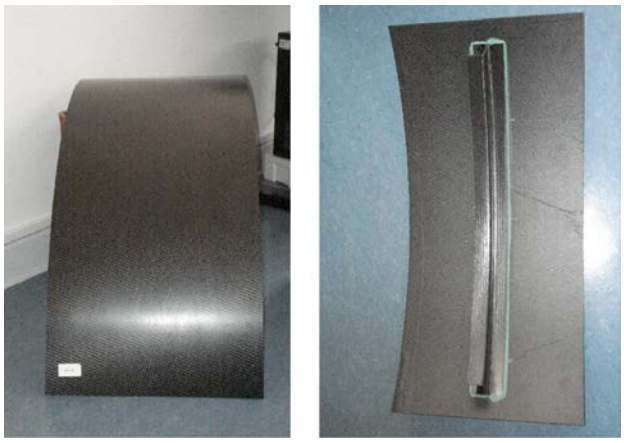

Figure 3: RTM Composite component assembly [10]

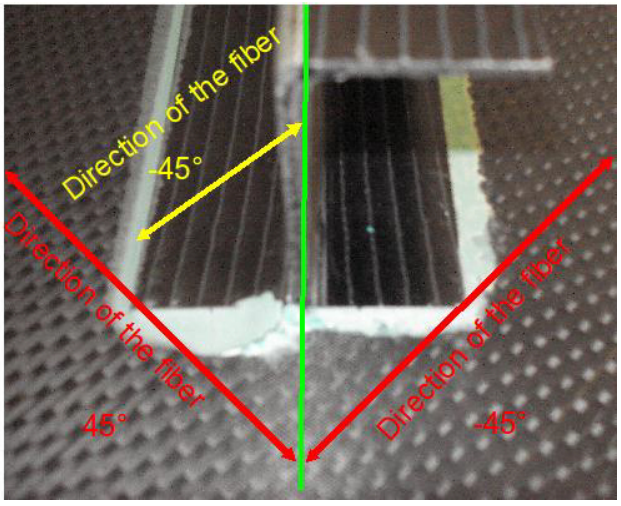

Figure 4: Composite component assembly detail [10].

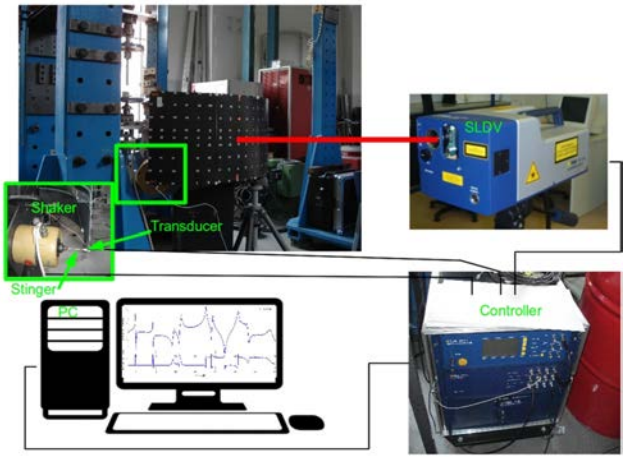

Figure 5: Experimental Set-up [11].

Ly 564 + Hexcel Gewebe G0926 (HTA-Faser) with dimensions of 0.390m × 0.810m (Figure 3 front and back part).

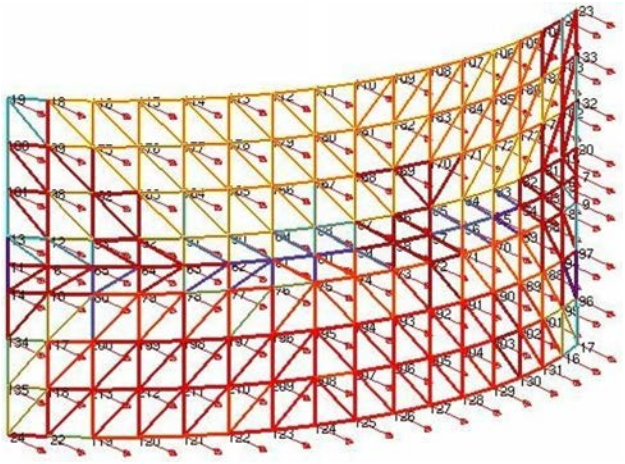

Figure 6: 153 Y-direction sensors [10].

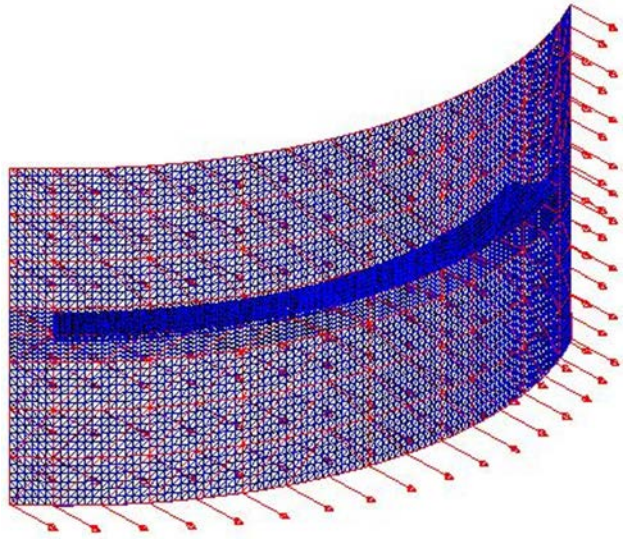

Figure 7: 153 Sensors in the FEM model [10].

The middle shell that connects the two principal parts with epoxic (Figure 4 has dimensions of 0.710m × 0.030m. Finally, there is the C-section Hexcel RTM6 + Saertex Multi-Axial-Gelege (MAG) with a IM7-Faser with dimensions of 0.710m × 0.030m. All the parts have symmetric layer distribution $[45/-45/45/-45/]_S$. All the measurements were performed with the Scanning Laser Doppler Vibrometer (SLDV) PSV840 by suspending the CFRP component from very soft cords (free condition), (see Figures 5-7).

The shaker LDS V406 and the stinger with length of 65 mm at node 17 are used to excite the structure that produce a sinusoidal vibration velocity signal on the line of sight of the SLDV (out-of-plane). The reason to use a stinger is to ensure that the shaker will only impart force to the structure along the axis of the stinger. The excitation signal selected is a periodic chirp (with frequency span 30-400

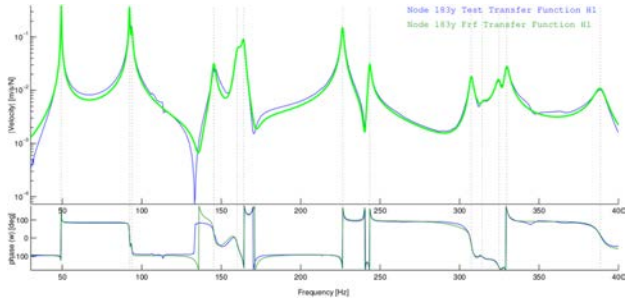

Figure 8: FRF(blue) and fitting curve (green) of composite model at node 183y [10].

Hz, 6400 lines of resolution, with complex average type and number of average per Frequency Response Function (FRF) equal to 10) and reflective foil is used to acquire the response measurement location. The input force is measured using a force transducer Dytran 1051V3 and power amplifier LDS PA 100 in order to record the excitation in the transverse direction. The interpolation between the experimental measurements uses FRFs [21]. The FRF, (see Figure 8), allowed us to compare the experimental modal parameters (frequency, damping, and mode shape) with the FE model. The Fast Fourier Transform (FFT) is a fundamental procedure that isolates the inherent dynamic properties of a mechanical structure and in our case with respect to the full FE models. To approximate the measurements (blue line) through a polynomial function (green line), it was used the frequency domain identification of structural dynamics applying the pole/residue parameterization [21], (see Figure 8). The experimental measurements were performed at low frequency (up to 400 Hz), and the curve-fitting generated from the experimental measurements [10]. A bandwith of 2% is used to localize the eigenfrequencies.

The CFRP provided by the DLR Braunschweig was measured, elaborated the FEM model and imported into SDTools using primarily triangular shells in the mesh (pshell). An appropiate assessment was perfomed to evaluate the mesh density of the FE model. Normal modes were computed using the FE model to obtain the natural frequencies and normal mode shapes of a CFRP structure. The model was divided in three parts, (see Figure 9), for convienience to modify the physical parameters per group of elements. The FE model is composed by triangular elements with a fairly regular shape and pattern.

A good practice in modal analysis using FE model assemblies is to couple the components using rigid body elements (RBE) or couplings as a boundary conditions to perform a modal analysis in the assembly. In this work, the FE model is prepared as a continuous body between

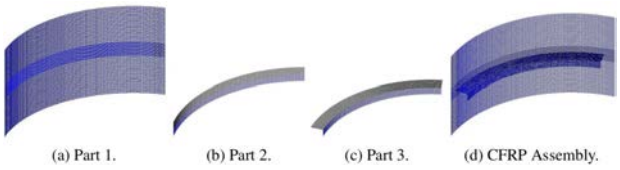

Figure 9: FEM groups.

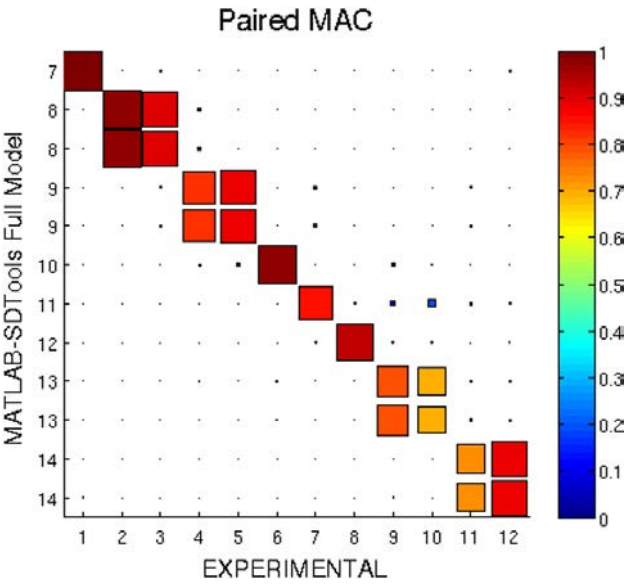

Figure 10: MAC: SDTools vs. Exp. [10]

the three components for convienience to simplify the FE model. The number of nodes and elements per group are listed in Table 3. After the FE model was developed, a number of validity checks were performed on the model prior to conduct the modal analysis. These check ups are units, mass comparation, layer stack-up, material and element properties and input and output coodinate systems.

The MAC analysis of the full FE model can be observed in Figure 10 (SDTools-MATLAB model versus the experimental measurements). The same number of modes was calculated in the full FE model. It was performed a cross orthogonality MAC (XOR) to verify the approximation of the full in low frequency range (12 mode pairs) versus the full model, see [10]. A good MAC correlation was obtained between updated full FE model and the experimental measurements in [10]. The nearly double correlation in the experimetal results identified in Figure 10 for the full models suggest the presence of the veering phenomena [23–25] (bending and torsional mode at the same frequency) in our composite component assembly. Thus, lower MAC results in 4,9,10 and 11 paired modes (see Figure 10) were archieved and identified using the experimental results.

Table 2: Comparative MAC: Updated full model (SDTools) and MSE results vs. experimental measurements.

ID	Test (Hz)	ID	FE model SDTools (Hz)	DF/FA %	MAC	ID	MAC MODAL /SEREP	MAC STATIC	MAC DYNAMIC	MAC MDRE	MAC MDRE-WE
1	49.243	7	57.218	16.2	100	1	100	100	100	100	100
2	92.265	8	106.02	14.9	97	2	99	100	100	100	99
3	93.756	8	106.02	13.1	90	3	98	100	100	100	99
4	145.29	10	168.2	15.8	83	4	99	100	100	100	99
5	160.05	10	168.2	5.1	86	5	100	100	100	100	99
6	164.18	9	167.5	2.0	98	6	100	100	100	100	99
7	226.36	12	236.83	4.6	86	7	99	100	100	100	99
8	243.4	11	234.99	−3.5	96	8	99	100	100	100	99
9	307.33	14	323.93	5.4	81	9	99	100	100	100	99
10	314.18	14	323.93	3.1	66	10	97	100	100	100	99
11	324.83	13	315.26	−2.9	74	11	94	100	100	100	99
12	329.67	13	315.26	−4.4	90	12	99	100	100	100	99

Table 3: FE model — elements, nodes and DOFs

Component	Element Type	Number of Elements	Number of Nodes
Part 1	pshell	7,200	3,840
Part 2	pshell	2,016	1,105
Part 3	pshell	3,024	1,615
Assembly		12,240	6,283
Total DOF			37,698

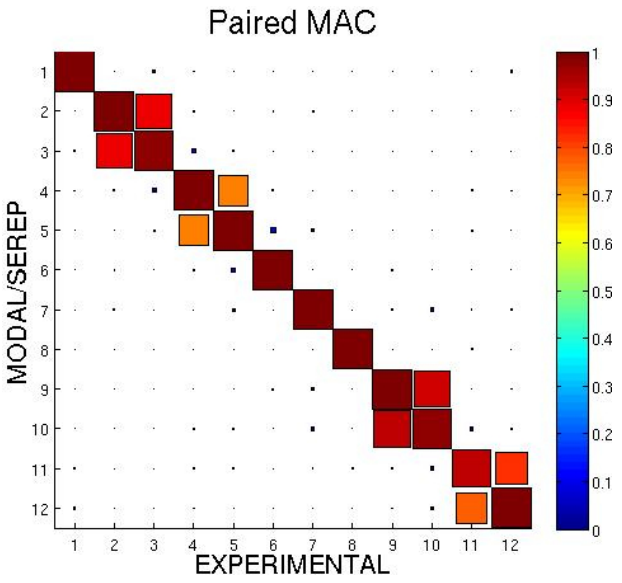

Figure 11: MAC: MSE MODAL/SEREP vs. Exp.

Furthermore, the different MSE are calculated (MODAL / SEREP, STATIC, DYNAMIC, MDRE, MDRE-WE)

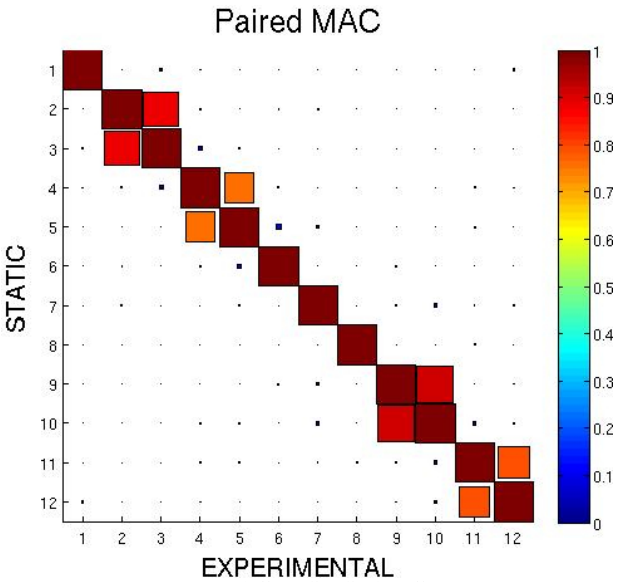

Figure 12: MAC: MSE STATIC vs. Exp.

based on the updated full FE model, the experimental measurements and curve-fitting according the methodology implemented in [29] using fe_exp command, (see Figures 11-15). The same number of paired modes are calculated (12 pairs) for all the MSE methods. An error of 0.1 is used in the interpolation of the MDRE-WE. In Figures 11-15, an improvement of the double correlation is identified using the MSE methods versus the experimental measurements.

The same number of DOF are obtained applying the MSE interpolation based on MOR methods according the number of DOF defined in the full model (37,698 DOF). In

Table 4: Comparative MAC: Updated full model (SDTools) and K-MAC MSE results vs. experimental measurements.

ID	Test (Hz)	ID	FE model SDTools (Hz)	DF/FA %	MAC	ID	K-MAC MODAL /SEREP	K-MAC STATIC	K-MAC DYNAMIC	K-MAC MDRE	K-MAC MDRE-WE
1	49.243	7	57.218	16.2	100	1	98	31	31	31	100
2	92.265	8	106.02	14.9	97	2	96	74	74	58	95
3	93.756	8	106.02	13.1	90	3	92	51	51	38	78
4	145.29	10	168.2	15.8	83	4	88	81	81	45	89
5	160.05	10	168.2	5.1	86	5	87	84	84	49	87
6	164.18	9	167.5	2.0	98	6	94	89	89	56	99
7	226.36	12	236.83	4.6	86	7	88	79	79	49	89
8	243.4	11	234.99	−3.5	96	8	96	89	90	65	97
9	307.33	14	323.93	5.4	81	9	88	81	81	60	87
10	314.18	14	323.93	3.1	66	10	79	65	66	45	76
11	324.83	13	315.26	−2.9	74	11	87	70	71	16	33
12	329.67	13	315.26	−4.4	90	12	93	87	88	39	89

Table 5: Comparative MAC: Updated full model (SDTools) and M-MAC MSE results vs. experimental measurements.

ID	Test (Hz)	ID	FE model SDTools (Hz)	DF/FA %	MAC	ID	M-MAC MODAL /SEREP	M-MAC STATIC	M-MAC DYNAMIC	M-MAC MDRE	M-MAC MDRE-WE
1	49.243	7	57.218	16.2	100	1	100	3	100	100	100
2	92.265	8	106.02	14.9	97	2	99	4	98	98	99
3	93.756	8	106.02	13.1	90	3	93	2	92	92	93
4	145.29	10	168.2	15.8	83	4	83	8	82	82	86
5	160.05	10	168.2	5.1	86	5	86	5	86	86	88
6	164.18	9	167.5	2.0	98	6	98	11	98	97	99
7	226.36	12	236.83	4.6	86	7	83	2	82	81	86
8	243.4	11	234.99	−3.5	96	8	96	86	96	96	98
9	307.33	14	323.93	5.4	81	9	82	5	80	78	83
10	314.18	14	323.93	3.1	66	10	69	2	65	64	70
11	324.83	13	315.26	−2.9	74	11	80	49	73	60	71
12	329.67	13	315.26	−4.4	90	12	90	2	89	83	91

Table 2 can be observed the improvement of the MAC values in all the paired modes of the MSE based on MOR versus the experimental measurements. The MAC values of the full FE model versus the experimental measurements can be observed in the left part of the Table 2.

Furthermore, the influence of the MOR methods using MSE can be analyzed obtaining the K-MAC and M-MAC displayed in Tables 4 and 5 respectively. The best K-MAC results are obtained applying the MODAL and MDRE-WE MSE methods displayed in Table 4. The worst paired modes of the MODAL and MDRE-WE MSE methods are displayed at paired mode 10 (K-MAC of 79) and at paired mode 11 (K-MAC of 33) respectively. The others MSE methods display a decrease of the K-MAC respect to the MODAL and MDRE-WE results. Furthermore, in Tables 2 to 5 are not displayed the differences of the eigenfrequencies between the experimental measurements and MSE results because there differences are zero.

There is a null difference in the frequencies applying different MSE because it is used the same pole identification obtained with the curve-fitting for all the MSE methods defined in [29]. The M-MAC of all the MSE methods can be observed in Table 5. A strong influence of the M-MAC results is observed in the subspace based expansion methods with the exception of the STATIC MSE method (the STATIC MOR is not taking in consideration the inertial forces). Using the contrieved example (modifying only the Young 's modulus E_1 and E_2 for all the three parts in the

Table 6: Comparative MAC: Contrieved full model (SDTools) and MSE results vs. experimental measurements.

ID	Test (Hz)	ID	FE model SDTools (Hz)	DF/FA %	MAC	ID	MAC MODAL /SEREP	MAC STATIC	MAC DYNAMIC	MAC MDRE	MAC MDRE-WE
1	49.243	7	64.497	31.0	100	1	100	100	100	100	100
2	92.265	8	117.86	27.7	97	2	99	100	100	100	99
3	93.756	8	117.86	25.7	90	3	98	100	100	100	99
4	145.29	10	184.66	27.1	61	4	99	100	100	100	99
5	160.05	10	184.66	15.4	88	5	100	100	100	100	99
6	164.18	9	177.54	8.1	81	6	100	100	100	100	99
7	226.36	12	257.19	13.6	47	7	99	100	100	100	99
8	243.4	11	257.19	5.7	55	8	99	100	100	100	99
9	307.33	14	344.15	12.0	66	9	99	100	100	100	99
10	314.18	14	344.15	9.5	49	10	97	100	100	100	99
11	324.83	13	340.81	4.9	64	11	94	100	100	100	99
12	329.67	13	340.81	3.4	73	12	99	100	100	100	99

Table 7: Comparative MAC: Contrieved full model (SDTools) and K-MAC MSE results vs. experimental measurements.

ID	Test (Hz)	ID	FE model SDTools (Hz)	DF/FA %	MAC	ID	K-MAC MODAL /SEREP	K-MAC STATIC	K-MAC DYNAMIC	K-MAC MDRE	K-MAC MDRE-WE
1	49.243	7	64.497	31.0	100	1	98	33	33	33	100
2	92.265	8	117.86	27.7	97	2	96	74	74	62	96
3	93.756	8	117.86	25.7	90	3	93	52	53	41	81
4	145.29	10	184.66	27.1	61	4	66	60	60	36	66
5	160.05	10	184.66	15.4	88	5	91	85	85	54	91
6	164.18	9	177.54	8.1	81	6	79	74	74	48	82
7	226.36	12	257.19	13.6	47	7	52	46	46	29	53
8	243.4	11	257.19	5.7	55	8	58	52	53	39	58
9	307.33	14	344.15	12.0	66	9	72	65	66	49	71
10	314.18	14	344.15	9.5	49	10	59	48	49	34	57
11	324.83	13	340.81	4.9	64	11	77	61	62	15	33
12	329.67	13	340.81	3.4	73	12	75	69	70	32	73

full FE model, $E_1 = E_2 = 97.3$ GPa), a decrese of the eigenvectors per paired mode as well as of the eigenfrequencies of the full FE model can be observed applying the MAC in the paired modes 4,6-12 in Figure 16 and Table 6, column (DF/FA). Furthermore, the MAC obtained in Figure 16 is used to calculate the MSE results modifying the E_1 and E_2 stiffness parameters. A good eigenvector correlation between the MSE and the experimental measurements can be observed between Tables 2 and 6 evaluating the stiffness parameters of the contrieved example respect to the updated stiffness parameters. Howerver, it can be identified the difference in the eigenvector correlation using the contrieved stiffness parameters. The MAC results in Table 6 suggest a robustness in the interpolation using MSE methods even though the MAC results of the contrieved full FE model displayed poor results, see Figure 16. However, the influence of the MOR methods using MSE methods can be analyzed using the K-MAC and M-MAC criteria. A negative impact in K-MAC and M-MAC is displayed in Tables 7 and 8 respectively using the stiffness parameters of the contrieved example. In Table 7 can be observed that the K-MAC results displayed a significative decrease in all the paired modes applying the different MSE methods respect to the K-MAC results displayed in Table 4. The STATIC, DYNAMIC and MDRE MSE methods display similar K-MAC and M-MAC values in the paired modes 1-3 in Tables 7 and 8 respect to the same paired modes in Tables 4 and 5 respectively. However, the rest of the paired modes obtained in

Table 8: Compartive MAC: Contrieved full model (SDTools) and M-MAC MSE results vs. experimental measurements.

ID	Test (Hz)	ID	FE model SDTools (Hz)	DF/FA %	MAC	ID	M-MAC MODAL /SEREP	M-MAC STATIC	M-MAC DYNAMIC	M-MAC MDRE	M-MAC MDRE-WE
1	49.243	7	64.497	31.0	100	1	100	2	100	100	100
2	92.265	8	117.86	27.7	97	2	99	3	98	98	99
3	93.756	8	117.86	25.7	90	3	94	1	92	92	93
4	145.29	10	184.66	27.1	61	4	62	5	61	60	62
5	160.05	10	184.66	15.4	88	5	89	5	89	89	90
6	164.18	9	177.54	8.1	81	6	83	18	83	83	84
7	226.36	12	257.19	13.6	47	7	49	1	48	47	50
8	243.4	11	257.19	5.7	55	8	57	54	56	56	57
9	307.33	14	344.15	12.0	66	9	67	3	65	65	68
10	314.18	14	344.15	9.5	49	10	52	1	50	49	52
11	324.83	13	340.81	4.9	64	11	70	48	65	57	64
12	329.67	13	340.81	3.4	73	12	73	1	72	69	74

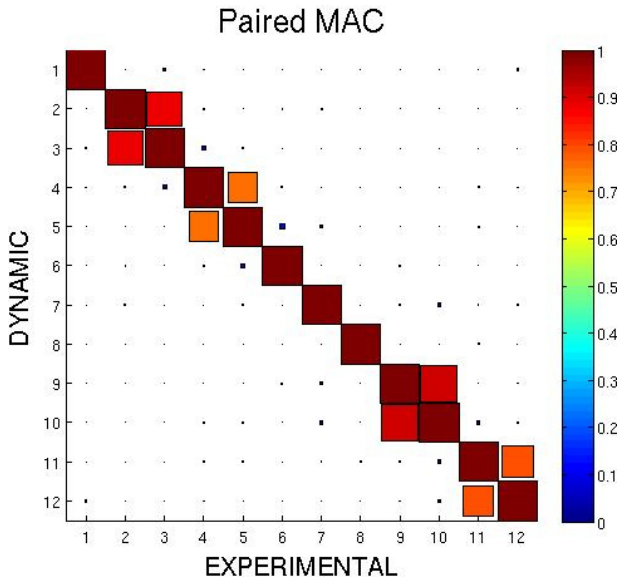

Figure 13: MAC: MSE DYNAMIC vs. Exp.

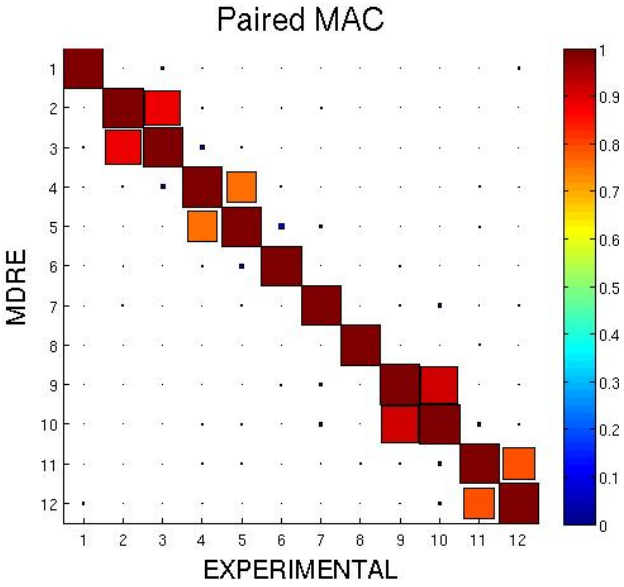

Figure 14: MAC: MSE MDRE vs. Exp.

Tables 7 and 8 using the K-MAC and M-MAC applying different MSE methods display a deterioration respect to the K-MAC and M-MAC results of Tables 4 and 5, with exception of the paired mode 5 with value of 91 in the K-MAC applying the MODAL and MDRE-WE MSE methods.

3.1 Conclusions

The application of MSE based on MOR methods using CMS to a CFRP component have shown good predictive capabilities of the dynamic behaviour in a CFRP combining experimental results, curve-fitting and an updated FE model. The experimental measurements performed with a SLDV and the identification of pole/residues used in a previous work are suitable to apply MSE methods to a CFRP according the results. It was observed an improvement in the MAC results between the experimental measurements and the MSE methods using the updated or modifying the stiffness parameters of the full model(contrieved model). However, the influence of the MOR using MSE can be identified comparing of K-MAC and M-MAC results (eigenfrequencies and eigenvectors) based on the modification of the stiffness parametes of the updated FE model. It is no-

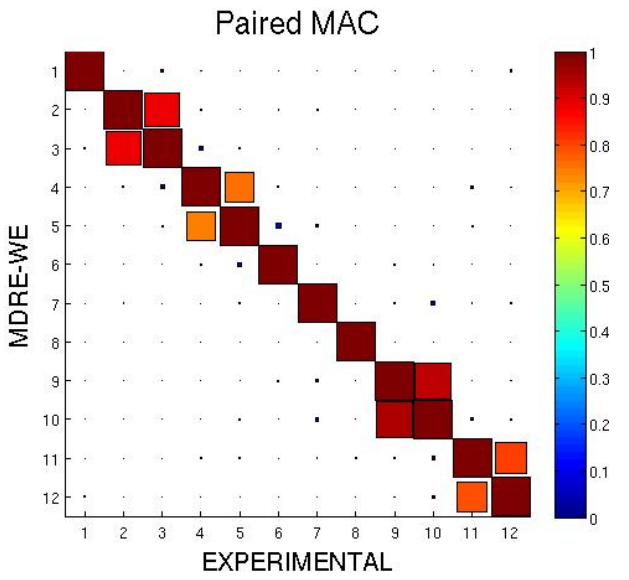

Figure 15: MAC: MSE MDRE-WE vs. Exp.

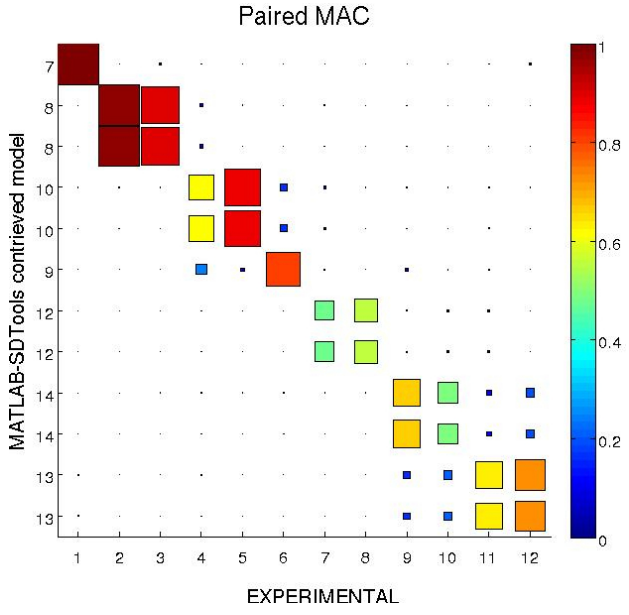

Figure 16: MAC: Contrieved vs. Exp.

ticed a strong influence of the stiffness parameters in the K-MAC and M-MAC criteria using MSE methods to a CFRP based on the MAC correlation between the experimental measurements and the full FE model. The best K-MAC and M-MAC results are observed using the MODAL/SEREP and MDRE-WE MSE methods implemented in SDTools based on the experimental measurements, curve-fitting and updated stiffness parameters obtained in a previous work. The strong influence of the stiffness parameters suggests that the distorsion of the subspace based expansion methods can be controlled applying the K- MAC and M-MAC using the MAC criteria. Furthermore, the general framework methodology of Ritz vectors, the updated stiffness parameters of the CFRP, the quality of experimental measurements, the curve-fitting algorithms based in the classical Laplace method and the type of element selected played an essential role in the dynamic correlation applying MSE, MOR and CMS methods to a CFRP.

Acknowledgement: This work has been supported by the DAAD-CONACYT Mexico with DAAD number: A/09/72544 and CONACYT Mexico number: 211983/306778. This support is gratefully acknowledged.

References

[1] Balmès E., Billet, L., Using expansion and interface reduction to enhance structural modification methods. IMAC XIX, 2001, 615-621

[2] Balmès E., Modes and regular shapes. How to extend component mode synthesis theory, XI DINAME, 28th February-4th March 2005, 1-14

[3] Balmès E., Review and Evaluation of shape expansion methods, IMAC 2000, 555-561

[4] Balmès E., Optimal Ritz vectors for component mode synthesis using singular value decomposition, AIAA J., 34(5), 1996, 1256-1260

[5] Maia N., Silva J., Theoretical and experiemental modal analysis, Mechanical engineering research studies, Engineering dynamics series, Research Studies Press, First edition, 1997

[6] Corus M., Balmès E., Improvement of structural modification method using data expansion and model reduction techniques. IMAC, 2003, pp. 1-7.

[7] Urgueia A., Using the SVD for the selection of independent connetions coordinates in the coupling of substructures. IMAC 1991, 919-925

[8] Balmès E., Sensors, degrees of freedom, and generalized mode-shape expasion methods, IMAC 1999, 628-634

[9] Balmès E., Use of generalized interface degrees of freedom in component mode synthesis, IMAC 1996, 204-210

[10] Peredo Fuentes H., Zehn M., Application of the Craig-Bampton model order reduction method to a composite component assembly: MAC and XOR, Facta Universitatis, series: Mechanical Engineering, 12(1), 2014, 37-50

[11] Peredo Fuentes H., Zehn M., Application of the Craig-Bampton model order reduction method to a composite component assembly: MACCO, COMAC, S-COMAC and ECOMAC, Open Eng.,6, 2016, 1-13

[12] Kammer D., Testing-analysis model development using an exact modal reduction, International Journal of Analytical and Experimental Analysis, 174-179

[13] O'Callahan J., Avitabile P., and Riemer R., System equivalent reduction expansion process (SEREP), IMAC VII, 1989, 29-37

[14] Guyan R., Reduction of Mass and Stiffness Matrices, AIAA Journal, 3, 1985, 380

[15] Kidder R., Reduction of structural frequency equations, AIAA Journal, 11(6), 1973
[16] Kammer D., A hybrid approach to test-analysis model development for large space structures, Journal of vibrations and acustics, 113(3), 1991, 325-332
[17] Roy N., Girard A. And Bugeat L.-P. Expansion of experimental modeshapes – An improvement of the projection technique, IMAC 1993, 152-158.
[18] Roy N., Girard A., Impact of residual modes in structural dynamics, Proceedings, European Conference of Spacecraft Structures, Materials & Mechanical Testing, Noordwijk, The Netherlands, 2005
[19] Ewins D. J., Modal testing: Theory and practice, Research Studies Press, Letchworth, U. K., 1995
[20] Gade S., Moller N.B., Jacobsen N.J., and Hardonk B., Modal analysis using a scanning laser Doppler vibrometer, Sound and Vibration Measurements A/S, 2000, 1015-1019
[21] Balmès E., Frequency domain identification of structural dynamics using the pole/residue parametrization, IMAC 1996, 540-546
[22] Craig, R.J., Bampton, M., Coupling of substructures for dynamic analyses, AIAA J., 6(7), 1968, 1313-1319.
[23] Bonisoli E., Delprete C., Espoito M., Mottershead J. E., Structural Dynamics with conicident Eigenvalues: Modeling and Testing, Modal Analysis Topics, 3, Conferencing Proceedings of the Society for Experimental Mechanics Series 6, 2011, 325-337
[24] Pierre C., Mode Localization and eigenvalue loci of Bridges with Aeroeslastic effects, Journal of Engineering Mechanics 126(3), 1988, 485-502
[25] Mounier D., Poilane C., Bucher C., Picart P., Evaluation of transverse elastic properties of fibers used in composite materials by laser resonant ultrasound spectroscopy, Proceeding of the acoustics 2012, Nantes Conference 23-27 April 2012, Nantes France
[26] Batoz J.L., Lardeur P., Composite plate analysis using a new discrete shear triangular finite element, International Journal for Numerical Methods in Engineering, 27, 1989, 343-359
[27] Batoz J.L., Bathe K.J., Ho L.W., A Study of three node triangular plate bending elements, International Journal for Numerical Methods in Engineering, 15, 1980, 1771-1812
[28] Batoz J.L., Lardeur P., A discrete shear triangular nine D.O.F element for the analysis of thick to very thin plates, International Journal for Numerical Methods in Engineering, 28, 1989, 533-560
[29] Balmès E., Structural dynamics toolbox and FEM-Link, User's Guide, SDTools, Paris, France, 2016, http://www.sdtools.com/help/sdt.pdf
[30] Schwarz, B.J., Richardson, M.H., Experimental modal analysis, CSI Reliability Week, Vibrant technology, 1(1), 1999, pp. 1-12.
[31] Formenti, D.L., Richardson M.H., Parameter estimation from frequency response measurements using rational fraction polynomials, IMAC 1st, 1982, pp. 1-8.
[32] Richardson, M.H., , Derivation of mass, stiffness and damping parameters from experimental modal data, Hewlett Packard Company, Santa Clara Division, 1, 1977, pp. 1-6.
[33] Richardson, M.H., Modal Mass, stiffness and damping, Vibrant Technology, Inc, 31, 2000, pp. 1-6.
[34] Richardson, M.H., Formenti, D.L., Global curve fitting of frequency response measurements using rational fraction polynomials, IMAC 3rd, 1985, pp. 1-8.